Study of a Novel Oscillating Surge Wave Energy Converter

Preprint

Michael Choiniere and Krish Thiagarajan
University of Maine

Nathan Tom
National Renewable Energy Laboratory

Presented at the Offshore Energy and Storage conference
Cape Cod, Massachusetts
July 12–14, 2017

NREL is a national laboratory of the U.S. Department of Energy
Office of Energy Efficiency & Renewable Energy
Operated by the Alliance for Sustainable Energy, LLC

This report is available at no cost from the National Renewable Energy Laboratory (NREL) at www.nrel.gov/publications.

Conference Paper
NREL/CP-5000-68763
August 2017

Contract No. DE-AC36-08GO28308

NOTICE

This report is available at no cost from the National Renewable Energy Laboratory (NREL) at www.nrel.gov/publications.

Available electronically at SciTech Connect http:/www.osti.gov/scitech

Available for a processing fee to U.S. Department of Energy and its contractors, in paper, from:

U.S. Department of Energy
Office of Scientific and Technical Information
P.O. Box 62
Oak Ridge, TN 37831-0062
OSTI http://www.osti.gov
Phone: 865.576.8401
Fax: 865.576.5728
Email: reports@osti.gov

Available for sale to the public, in paper, from:

U.S. Department of Commerce
National Technical Information Service
5301 Shawnee Road
Alexandria, VA 22312
NTIS http://www.ntis.gov
Phone: 800.553.6847 or 703.605.6000
Fax: 703.605.6900
Email: orders@ntis.gov

Cover Photos by Dennis Schroeder: (left to right) NREL 26173, NREL 18302, NREL 19758, NREL 29642, NREL 19795.

NREL prints on paper that contains recycled content.

Proceedings of Offshore Energy and Storage 2017
Cape Cod, Massachusetts, USA
July 12-14, 2017

Study of a Novel Oscillating Surge Wave Energy Converter

Michael A. Choiniere*
Department of Mechanical Engineering, University of Maine
5711 Boardman Hall Room 219, Orono, ME 04469, USA
Nathan M. Tom
National Renewable Energy Laboratory, MS 3811
15013 Denver West Parkway, Golden, CO 80401, USA
Krish P. Thiagarajan†
Department of Mechanical Engineering, University of Maine
5711 Boardman Hall Room 229, Orono, ME 04469, USA

Abstract

This study investigates the performance of an oscillating surge wave energy converter (OSWEC) that utilizes adjustable geometry as a means of controlling the hydrodynamic coefficients, a concept originally proposed by [1]. The body of the device consists of a bottom-hinged solid rectangular frame with five horizontal flaps spanning the interior of the frame. The flaps can rotate independently about their center of rotation within the frame like a large window shutter. Changing the orientation of the flaps alters the hydrodynamic coefficients and natural frequency of the device as well as the ability to shed or absorb structural loads accordingly. This ability may allow the device to operate in a wider range of sea states than other current wave energy converter designs. This paper presents and compares the results of numerical simulations and experimental testing of the OSWEC's response to regular waves with all five of the horizontal fin configurations sharing the same orientation of 0° (fully closed interior) and 90° (fully open). The numerical simulations were performed using WAMIT, which calculates hydrodynamic coefficients using a boundary element method code to solve the linear potential flow problem, and WEC-Sim, a MATLAB-based tool that simulates multibody devices in the time domain by solving the governing equations of motion. A 1:14 scale model of the device was built for experimental evaluation in an 8-m-long, 1-m wide wave tank, which supports a water depth of 0.7 m. The OSWEC motion in different wave conditions was measured with displacement sensors while nonlinear wave-structure interaction effects like slamming and overtopping were captured using a high-speed camera and used to understand differences between the simulation and experiments.

1. Introduction

In this paper, we study the performance of a bottom-hinged oscillating paddle with variable geometry. This concept was labeled as an oscillating surge wave energy converter (OSWEC) and studied in [1]. Coastal and nearshore wave energy converters (WECs), similar to the one proposed here, have been the subject of recent research, with concepts like the Oyster [2], Waveroller [3], and the surge WEC [4]. The uniqueness of the present concept is the ability to vary some geometrical features to optimize the power generation and shed hydrodynamic loads, subject to different field locations and environmental conditions. Fig. 1 shows a concept of the OSWEC studied in this work. The main body is a plate or a paddle with some thickness, which is hinged at the base and extends up to the mean water level, and is subject to the wave field incident normal to its surface. The main response of the plate is an oscillatory rotation (ϕ) about its hinge, and for still water conditions the paddle surface does not pierce the free surface, which contrasts with other similar studies, e.g., [5] and [6]. The flaps located in the lower part of the plate can, in principle, be adjusted to any angle (φ) about their axis of rotation. For the purposes of this study, the flap orientation was limited to the closed (0^o) and open (90^o) configurations only. This change in flap orientation is expected to change the structure's hydrodynamic properties and hence its performance as a wave energy extractor.

Starting from first principles, the equation of motion of the OSWEC can be written as:

$$J\ddot{\phi} = \sum M \quad \#(1)$$

where J represents the device's mass moment of inertia. The moments that comprise the right side of Eq. (1) are:

a. Hydrostatic restoring moment, which is the balance between the effects of gravity and buoyancy (Fig. 1) and for small angles, is given by: $M_h = (\rho g \forall z_b - W z_g)\phi$. Here ρ is the water density, g is acceleration

*Corresponding author, michael.choiniere@maine.edu
†Professor & Presidential Chair in Energy

due to gravity, ∀ is the submerged volume of the device, and W is its weight. z_b and z_g denote the vertical positions of the centers of buoyancy and gravity from the origin of reference, respectively. See Fig. 1.

b. Hydrodynamic torque, M_r, is comprised of an added inertia term and a drag term. The added inertia is represented often by an added mass moment of inertia coefficient (A_{55}), which will be determined by computational methods in this paper. The drag term is dependent on several factors, including friction, and form drag and radiation damping. The friction component is often found to be negligible in structures moving in water; see e.g., [5]. The form drag is composed of fluid damping arising from flow separation off the edges and through orifices and is often nonlinear with the amplitude of motion [5, 6]. The radiation damping arises from wave generation as a result of paddle movement. Hydrodynamic torque has been the subject of considerable discussion in [4]. In a linearized sense, the hydrodynamic radiation moment can be written as $M_r = -A_{55}\ddot{\phi} - B_{55}\dot{\phi}$, where B_{55} is the wave radiation damping coefficient.

c. Incident wave-induced moment, M_w, is a combination of the incident wave-induced pressure acting on the surface of the paddle, and the wave diffraction effect assuming that the paddle is stationary. These forces are normally determined from a numerical simulation, as described later in Section 3. For small amplitude waves, the moment is normally written as a linear function of the wave amplitude, A.

d. Structural damping, M_s, is a result of any friction in the bearings at the bottom hinge of the paddle as well as string potentiometers attached to the paddle in an experiment. The string potentiometers consist of a fixed case that contains a rotational transducer with an extendable stainless steel wire rope that attaches to the moving paddle. An internal torsional spring maintains a constant tension on the wire rope throughout its stroke and acts as the retraction mechanism. A lubricated dust wiper makes contact with the wire rope as it extends and retracts in and out of the case creating low friction on the paddle. These effects are usually written as the product of a damping coefficient (B_s) and the paddle velocity, and quantified by decay tests in air.

e. Power take-off (PTO) moment, M_{PTO}, caused by the power take-off system working to remove energy from the oscillating paddle, is normally written as the product of a damping coefficient (B_{PTO}) and the paddle velocity. For the purposes of this paper, the power take-off is not used in the experiments. However, some discussion on the effect of including a PTO in numerical simulations is included.

By combining these moments, the equation of motion can be rewritten as:

$$(J + A_{55})\ddot{\phi} + (B_{55} + B_s + B_{PTO})\dot{\phi} + (\rho g \forall z_b - W z_g)\phi = M_w \#(2)$$

This equation is a linearized version of the complete nonlinear formulation of the problem. Refer to the work of Gomes et al. [5], for a comprehensive treatment of the latter. If the far-field incident wave and the paddle motion response are assumed to be sinusoidal with frequency ω, and with amplitudes A and ϕ_0, respectively, then a nondimensional response amplitude operator (RAO) is calculated by:

$$RAO = \frac{\phi_0}{kA} \#(3)$$

where k is the wave number corresponding to the linear dispersion relation of progressive waves, and can be computed from the wave frequency and water depth.

Power capture efficiency provides important information in regards to evaluating the performance of the OSWEC. This concept is explored in this paper using the capture width, C_w, which is a ratio of the time-averaged power absorbed by the PTO, P_{TAP}, to the time-averaged power per unit width contained in the incident wave, P_w. From linear wave theory principles, P_w is obtained from [1]:

$$P_w = \frac{1}{4}\rho g A^2 \sqrt{\frac{g}{k}\tanh kd}\left[1 + \frac{2kd}{\sinh 2kd}\right] \#(4)$$

The capture width is nondimensionalized by dividing by the width of the device, w,:

$$C_w = \frac{P_{TAP}}{wP_w} \#(5)$$

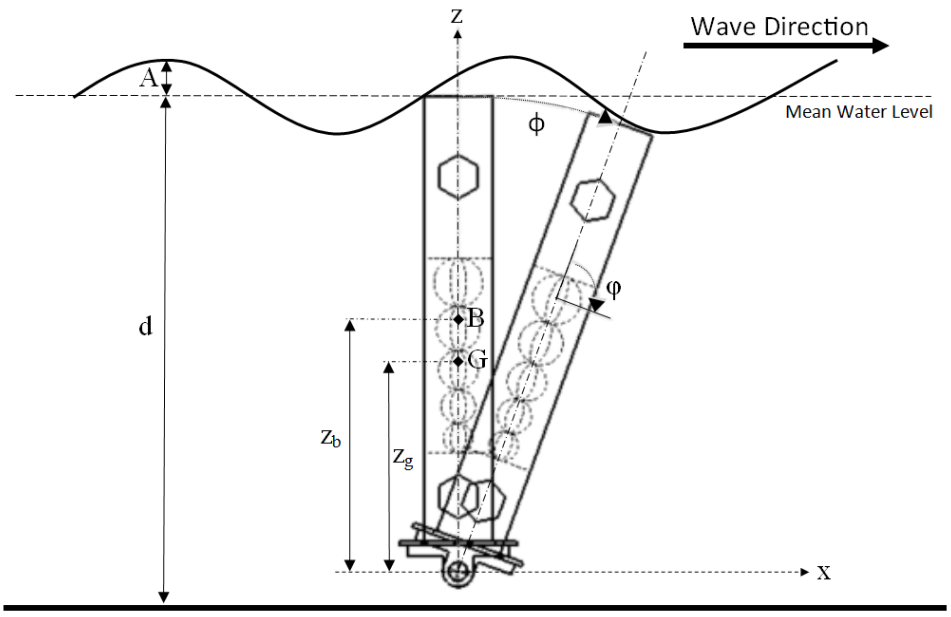

Figure 1. Sideview of OSWEC device and associated variables.

2. Model Description

The main paddle of the device under investigation was constructed from sheets of high-density polyethylene that were heat welded at the joints to create watertight, upper and lower hollow chambers connected by solid side plates. Both the upper and lower chambers contain PVC pipes that span the width of the device to act as ballast ports for future studies. These ports were empty and sealed with threaded caps for the current experiments. The main paddle body incorporated a window that housed the variable-pitch flaps. The five variable-pitch elliptical flaps were printed in three dimensions in sections of polylactic acid plastic with 40% infill. The individual sections of each flap were joined with two continuous wooden dowels through the interior of each section spanning the width of the window, and reinforcing strips of fiberglass on each broad side of the ellipse. A final coat of epoxy was applied to protect each flap from leaks. The minor axis dimension of each ellipse is constant at 21 mm whereas the major axis dimension varies with each flap as shown in Fig. 2.

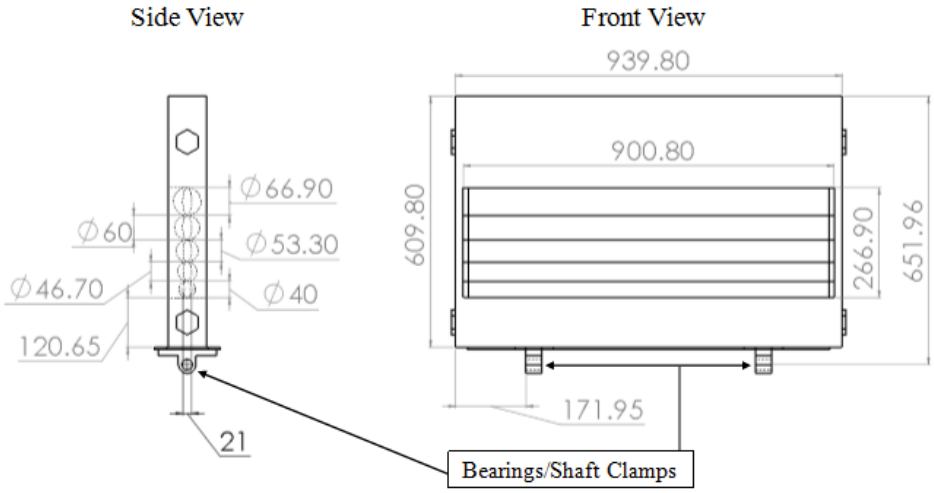

Figure 2. Dimensions of interest (mm) of the scale model OSWEC with variable flaps at φ = 0°.

The high-density polyethylene body was mounted to a steel bearing plate at its bottom surface, and utilized corrosion-resistant bearings with integrated shaft clamps at the locations shown in Fig. 2. Greater detail of the entire device is shown in Fig. 3. The OSWEC was mounted in the wave tank by a rigid frame made of ¼" by 3" steel flat bar that was clamped to the wave tank structure and hugged the tank walls and floor to create as little obstruction as possible. Finally, a 1-inch-diameter steel shaft connected the OSWEC to the frame through the bearings.

The OSWEC was free to oscillate about its axis of rotation (ϕ), and each flap was capable of rotating about its respective axis of rotation (φ). This convention is shown in Fig. 1.

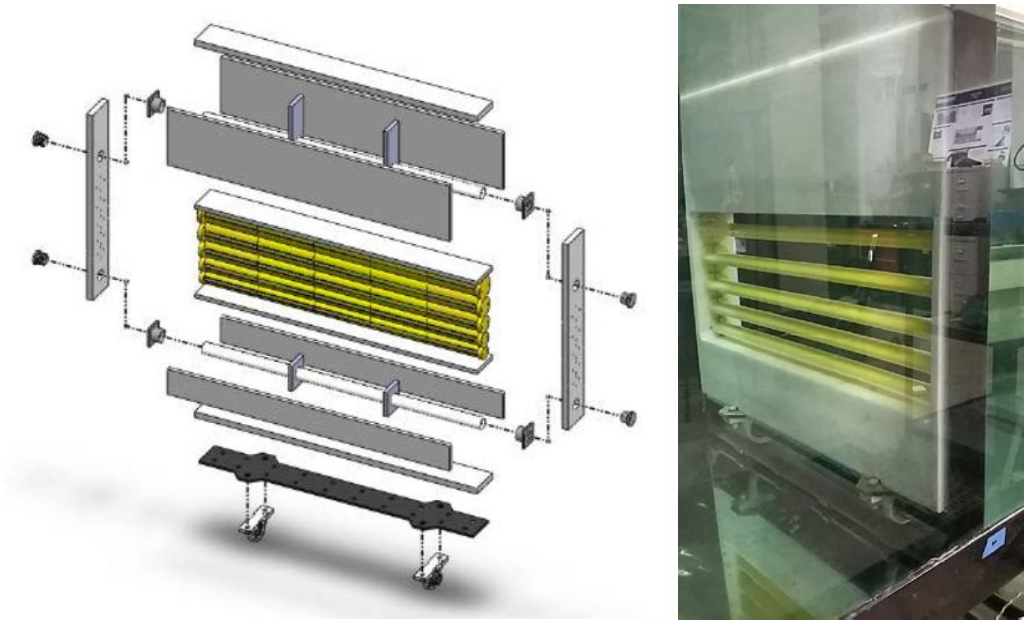

Figure 3. The OSWEC model exploded in assembly view (left) and the device installed in the wave tank (right).

3. Experimental Methodology

The OSWEC model was tested in an 8-m-long, 1-m-wide wave tank that supports a water depth of 0.7 m. Waves were generated by a vertically actuated wedge of 45° at one end of the tank and a porous beach at the other end to reduce the amplitude of reflected waves. The wave maker and tank can produce regular waves with periods ranging from 0.6 s to 2.0 s and wave amplitudes of 0.0033–0.0897 m.

The width of the OSWEC model was chosen specifically to span the width of the tank to simplify the analysis to two dimensions, assuming water particle motion would be limited to the *x*-*z* plane.

Prior to installing the OSWEC in the wave tank, wave heights were recorded in the open tank at a sample rate of 1 kHz. The geometry of the tank and motion of the wave maker resulted in small nonlinearities, and multiple harmonics in the measured wave elevation. Therefore, a fast Fourier transform was used to isolate the wave amplitude of the first harmonic in the data for each set of wave maker inputs.

Two opposing string potentiometers, each with a 1-m stroke, were used to measure the OSWEC's response in waves. The string potentiometers were mounted to the top tank rail support while the free ends of each string were attached to a vertical steel stanchion that was bolted to the side of the OSWEC. A schematic of the experimental setup is shown in Fig. 4, and a photo of the OSWEC and string potentiometer is shown in Fig. 5. Although the potentiometers measured a linear displacement and the height of the potentiometers above the axis of rotation, *H*, was constant, and given that the OSWEC would only be subject to small angular displacement, the rotational displacement, ϕ, of the device was calculated as:

$$\phi = \tan^{-1}\frac{\Delta x}{H} \#(6)$$

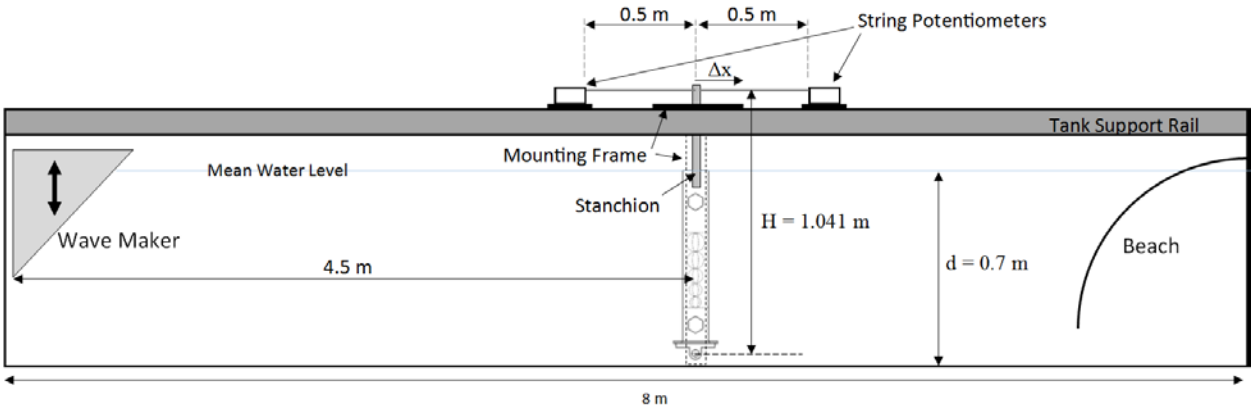

Figure 4. Wave tank and experimental setup (not to scale).

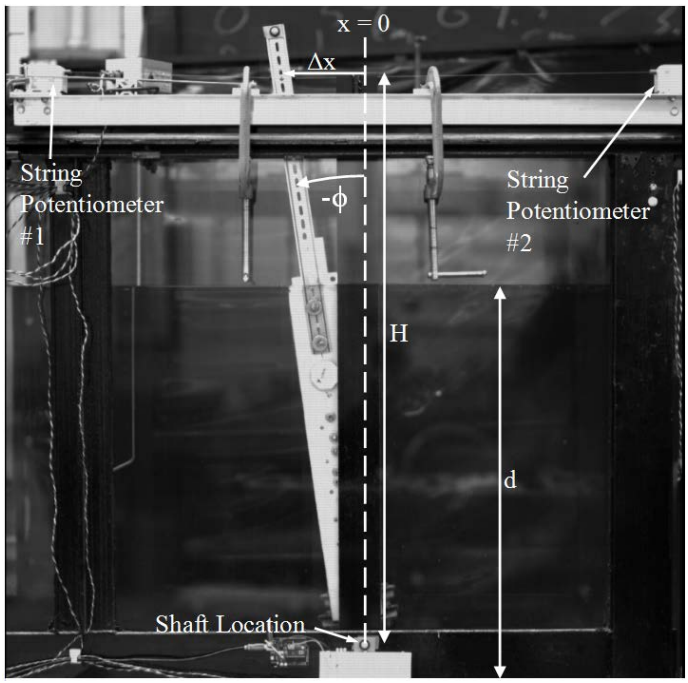

Figure 5. Instrumentation detail.

4. Numerical Simulation Details

The program selected to predict the OSWEC angular displacement during model tests was WEC-Sim [7]. WEC-Sim is an open-source wave energy converter simulation tool that is built on the MATLAB/SIMULINK framework and a collaboration between the National Renewable Energy Laboratory and Sandia National Laboratories. Simulations are performed in the time domain by solving the WEC equations of motion in all 6 degrees of freedom. Before WEC-Sim could be run, it was necessary to obtain the mass and hydrodynamic properties of the OSWEC. The translational mass, center of gravity, and mass moment of inertia were obtained from dry tests at the University of Maine's Advanced Structures & Composites Center. The hydrodynamic coefficients were obtained from WAMIT v7.2 [8], which now includes the option to analyze bodies in channels with parallel walls. The coefficients were calculated at a spacing of 0.1 rad/s for wave frequencies between 2.0 rad/s and 11.0 rad/s for the 0^o and 90^o flap orientations.

The first harmonic of the wave period and wave amplitude, measured during the open tank tests, were used as the environmental inputs to WEC-Sim. Simulations were run for 40 wave periods (40T) with a time step of T/100 and ramp up time of 10 wave periods (10T). WEC-Sim has two options to calculate the hydrodynamic radiation torque: 1) the sinusoidal steady-state response, which assumes that the added moment of inertia and the wave damping are

constant at the simulated wave frequency, and 2) with the full convolution integral. However, WAMIT currently does not calculate the infinite frequency added moment of inertia when using the channel option, which prevents implementation of option 2. As a result, option 1 was selected for initial comparisons.

A rotational constraint was used in WEC-Sim to model the connection between the OSWEC and the rigid frame shaft. The rotational constraint is required because WEC-Sim requires the mass and hydrodynamic properties to be defined about the center of gravity. It was assumed in the simulations that linear wave theory is applicable and no additional modeling features were used in WEC-Sim.

5. Results and Discussion

Free-decay experiments were performed to identify the damped natural period of the device. Five tests at each flap orientation were recorded and showed sufficient repeatability in response. As shown in Fig. 6, the 0° flap orientation exhibits an irregular decay curve. This irregular decay suggests that the device possesses nonlinear damping in this orientation, which is likely due to the tank geometry and proximity of the tank side walls and motion of the displaced water and its reflection. This characterization will be a priority in future work with this device.

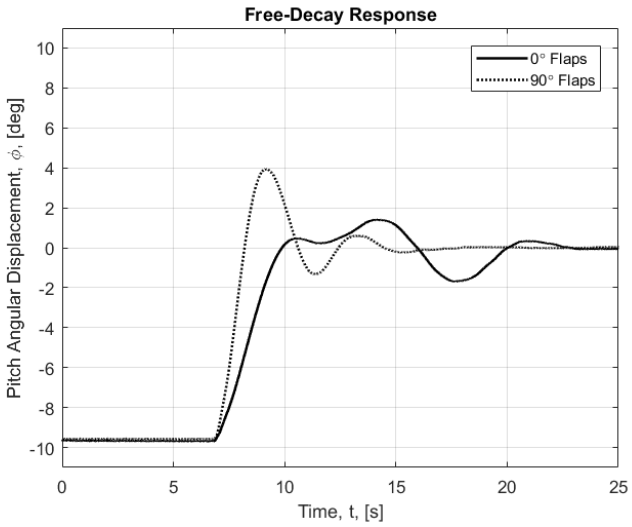

Figure 6. Free-decay response of the OSWEC at both 0° and 90° flap orientations.

The damped natural period between the second and third peaks of the 0° flap case was T_d = 6.73 s, and T_d = 4.11 s in the 90° case. Because the hydrostatic restoring coefficient and moment of inertia are constant with flap rotation, the reduction in the damped natural period confirms that the added moment of inertia has been reduced in the 90° case. Note that the wave maker used in the current experiments is limited to wave periods of 2 s or less, so the device's response was not examined in waves with periods near these damped natural periods. After scaling up from the 1:14 model results, the full scale these damped natural periods are equivalent to T_d = 25.18 s and T_d = 15.38 s, respectively.

Fig. 7 shows the surge hydrodynamic coefficients which have the greatest effect on the paddle pitch about the rotational shaft, the surge wave excitation force, and the pitch wave excitation moment which were calculated in WAMIT for the OSWEC modeled in a channel. The dimensionless frequency is defined as:

$$\omega^* = \frac{\omega}{\sqrt{g/d}} \#(7)$$

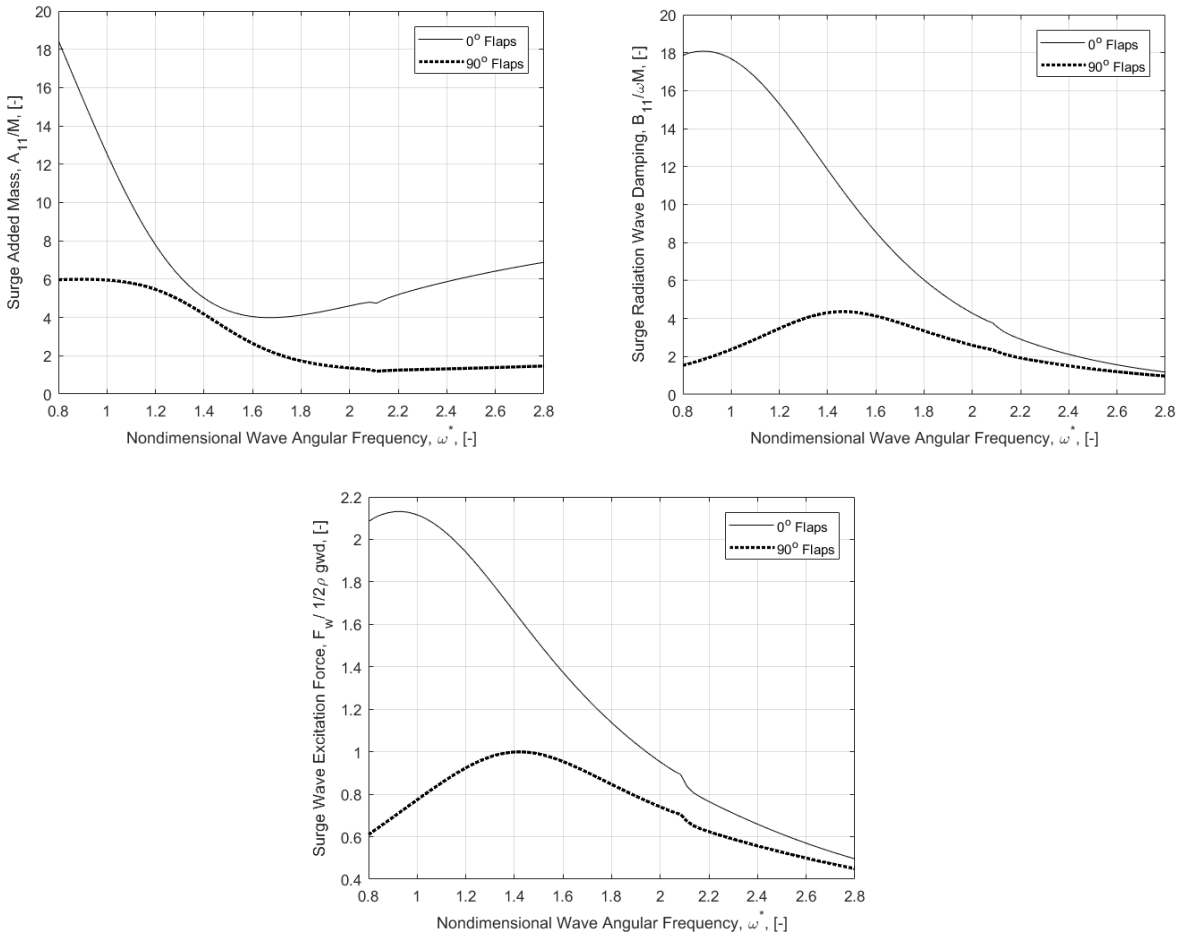

Figure 7. Surge added mass (top left), surge radiation wave damping (top right), and surge wave excitation force (bottom) as calculated by WAMIT. WEC-Sim requires the hydrodynamic coefficients to be calculated about the center of gravity of the WEC. After placing a revolute joint at the base of the OSWEC, to model the shaft connection, the dominant moment will be generated by the surge hydrodynamic coefficients.

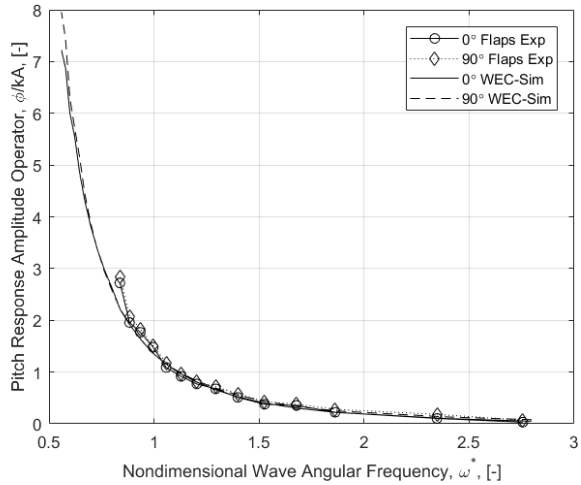

Figure 8. Pitch RAO calculated from experimental results and WEC-Sim results at both 0° and 90° flap orientations.

Much like the wave data collected prior to device installation, the OSWEC's response to incident waves exhibited small multiple harmonics in the angular displacement time history. To be consistent with the method used to characterize the incident wave amplitude, a fast Fourier transform analysis was also performed on the angular displacement time history collected in each run. The amplitude of the first harmonic was considered as the OSWEC's angular displacement amplitude and used to determine the pitch RAO. The experimental pitch RAO calculations are compared to the WEC-Sim results in Fig. 8.

The experimental free-decay test and the numerically derived hydrodynamic coefficients shown in Fig. 6 and 7 suggest that hydrodynamic properties and the resonant pitch frequency can be adjusted by changing flap orientation. Therefore, the response at each flap orientation was expected to show significant differences. However, Fig. 8 shows that the flap orientations investigated do not significantly influence the unforced (no PTO) OSWEC's pitch response in the environment studied. The experimental wave frequencies tested were likely high enough such that the hydrodynamic wave pressure did not penetrate to the depth of the flaps. The pitch response, however, shows good agreement between the numerical and experimental results, which provides validity to the calculated hydrodynamics.

The authors believe that the original two-dimensional assumption, where the model spans the width of the tank, may be a major contributor to the limited effect of flap orientation to response in this experiment. The broad upper face above the flap window of the OSWEC was designed to be nonadjustable as most of the incoming wave energy is in this area near the water surface. In the experimental environment, incident water particles are primarily restricted to flow over the device, but in a full-scale deployment with no channel (wall effects), particles would be free to flow around the device as well. Vortex shedding was also observed in the small space between the side of the OSWEC and the tank walls—especially on the 0° flap condition—which may have led to further limitations of flap orientation effects.

While the unforced pitch response in waves did not show significant changes between the 0° and 90° flap cases, the differences in free-decay response and hydrodynamic coefficients calculated in WAMIT warranted further investigation of the device's ability to extract energy and shed loads. A linear rotational PTO was added to the WEC-Sim model and simulations were performed for wave periods of 0.7, 1.0, 1.3, 1.6, and 1.9 seconds and PTO damping coefficients ranging between 25 and 425 $kg{\cdot}m^2{\cdot}s^{-1}$. The WEC-Sim results for the resistive torque applied by the rotational PTO, as a function of the PTO damping coefficient, are shown in Fig. 9.

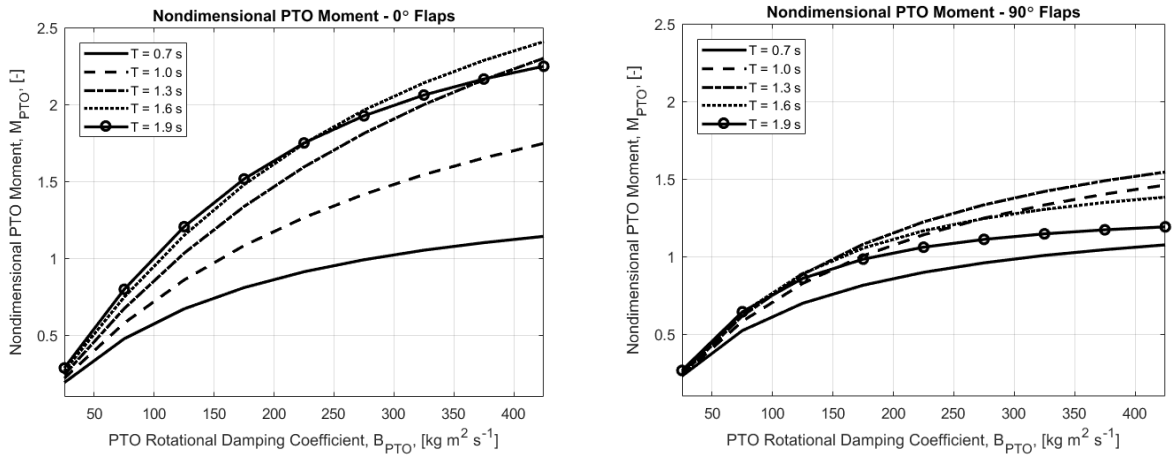

Figure 9. Nondimensional PTO moment over a range of PTO damping coefficients for both 0° (left) and 90° (right) flap orientations. The PTO moments are nondimensionalized by $\tau_m = 1/6\,\rho g w d^2 A$, where w is the width of the device. The resulting hydrostatic moment from having water on one side of the paddle is represented by τ_m.

Another factor that becomes increasingly important as the device approaches full-scale deployment is the load on its base or foundation. The surge foundation force was also examined in the WEC-Sim runs with the incorporated rotational PTO. The resulting nondimensional surge force on the supporting frame is shown in Fig. 10. Finally, the WEC-Sim with rotational PTO results were used to estimate the capture efficiency of the OSWEC at both the 0° and 90° flap orientations over the same range of PTO damping coefficients with results plotted in Fig. 11. The results

from WEC-Sim, shown in Fig. 9–11, demonstrate the ability of the adjustable flap orientation to control PTO and foundation loads.

The transfer of energy from wave to OSWEC was investigated further using data collected in the experiments explained earlier. Fig. 12 shows a time history of the wave field upstream and downstream of the device along with the OSWEC's pitch response for wave periods of 1.0 s and 1.6 s. The OSWEC was located at $x = 0\ m$ and the upstream and downstream wave probes were located at $x = -0.53\ m$ and $x = 0.60\ m$, respectively. The horizontal dashed lines represent the intended wave elevation at the paddle location had the device not been installed.

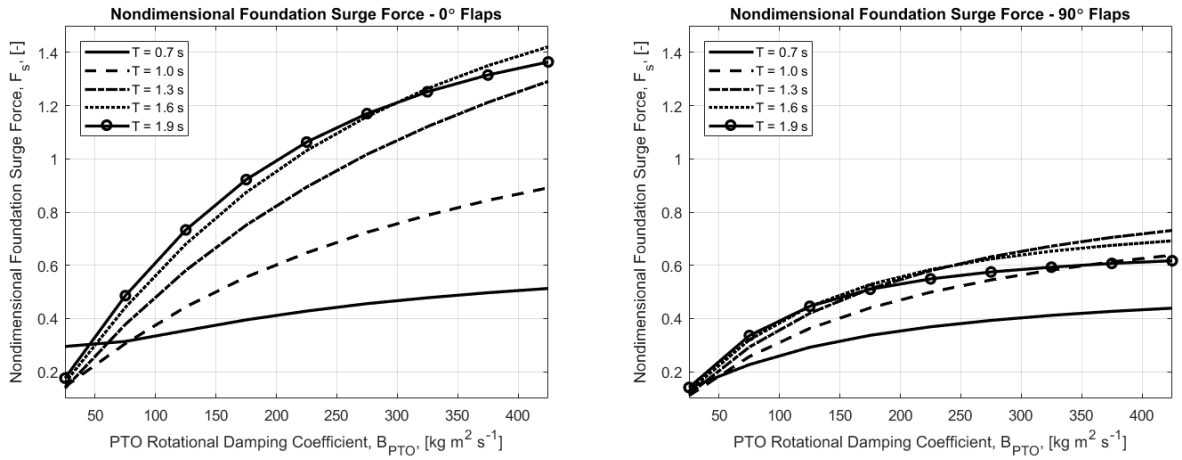

Figure 10. Nondimensional surge force on foundation over a range of PTO damping coefficients for both 0° (left) and 90° (right) flap orientations. The surge forces were nondimensionalized by $f_r = 1/2\,\rho g w d A$, where w is the width of the device. The resulting hydrostatic horizontal force from having water on one side of the paddle is represented by f_r.

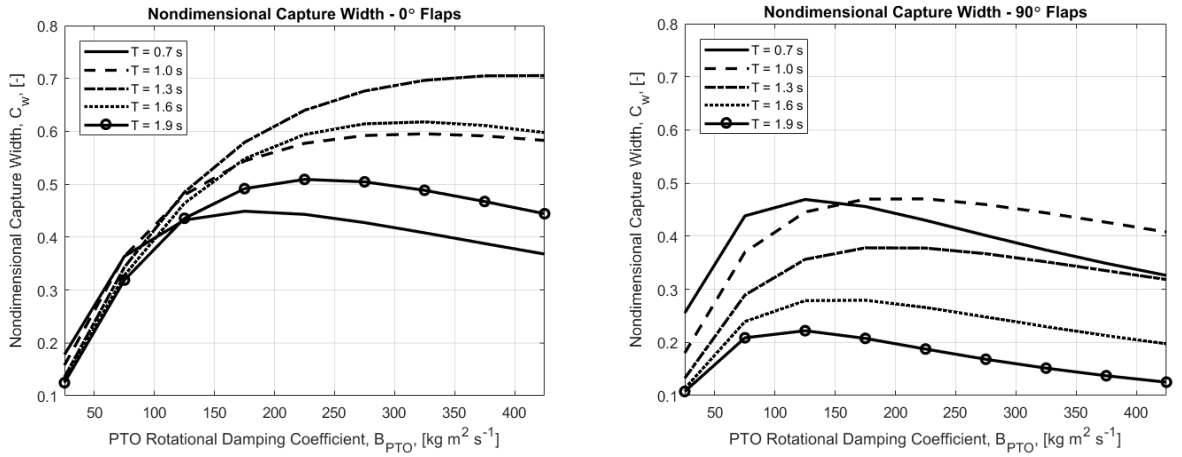

Figure 11. Nondimensional capture width over a range of PTO damping coefficients for both 0° (left) and 90° (right) flap orientations.

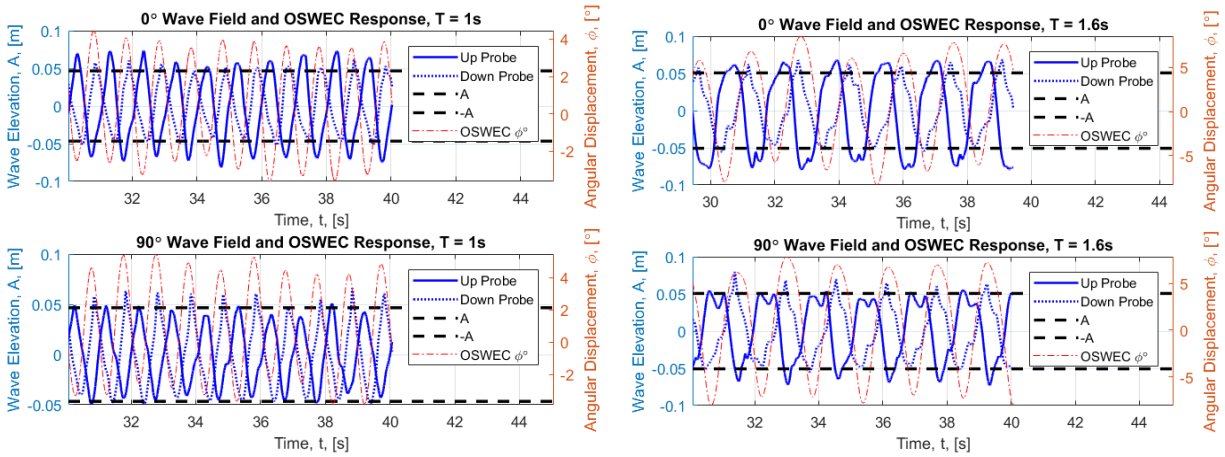

Figure 12. Time history of upstream and downstream wave elevation and OSWEC pitch response in waves of $T = 1.0\ s$ (left) and $T = 1.6\ s$ (right) for the 0° and 90° flap orientations.

The wave elevation at the upstream probe in each 0° case was greater than the 90° case for the same wave environment. This outcome was expected as the 90° case would allow some of the wave energy to pass through the openings in the flap window. Further, it indicates that the device reflects more energy back in the 0° case, which agrees with the increased capture width, foundation surge force, and PTO moment calculated from the WEC-Sim results in Fig. 9–11. Given this information, it would be expected that the 0° flap orientation would radiate a greater amount of energy in the downstream direction. However, the wave elevation at the downstream probe for each wave period does not appear to change between the 0° and 90° flap orientations. A high-speed camera was used during the experiments to capture nonlinear wave-structure interactions that would help identify differences between the experimental and numerical results. Fig. 13 shows an overtopping sequence that was recorded.

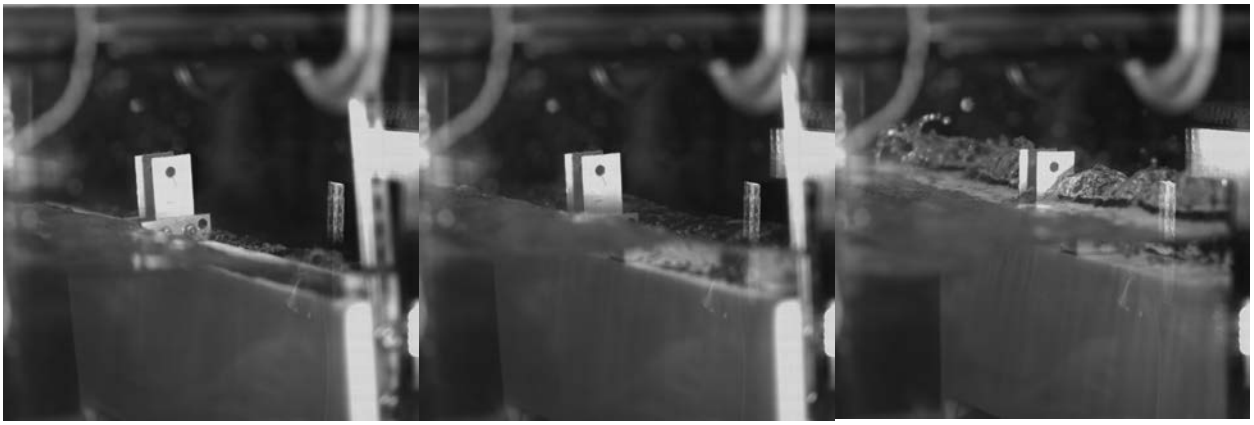

Figure 13. Overtopping sequence for wave period $T = 1.2\ s$ and wave amplitude $A = 0.07\ m$ and the device in the 90° flap orientation. Images were recorded at a capture rate of 500 frames per second.

As the wave passes the OSWEC, the radiated energy on both sides of the paddle can be seen in Fig. 13 as the wave appears to split over the device. Some of the transmitted wave energy is dissipated as the elevated water on each side of the paddle finally collides and projects vertically, as shown in the third frame of Fig. 13. This vertical projection of the wave surface is a possible explanation for the similarity in transmitted energy between the two flap orientations at the downstream probe in Fig. 12. Another explanation may be that the waves investigated may have been of sufficiently high frequency in which the wave pressure may not penetrate below the solid upper panel, resulting in radiated wave energy that is greater than the energy transmitted.

6. Conclusions

This paper investigated the performance of an oscillating surge wave energy converter utilizing adjustable flaps as a means of controlling the hydrodynamic loads. The pitch response to waves was measured experimentally for flap orientations of 0° and 90°. The experimental conditions were modeled numerically using WAMIT and WEC-Sim and a good agreement was found between the simulations and experiments. Flap orientation did not have a significant effect on angular displacement of the device when the PTO was absent, so further numerical simulations were performed to estimate the effect of flap orientation on structural loads and power capture. The numerical results suggest that when partnered with traditional PTO damping control strategies, the adjustable geometry adds a significant layer of control and tuning capabilities that warrant further optimization studies.

Future updates for this conceptual device include testing in a much larger wave basin in the absence of wall effects and with the ability to generate longer wave periods. It is of interest to observe the model's response to wave periods on both sides of its resonant pitch period and the effect of flap orientation to a wider range of environmental conditions. Repeating free-decay tests in an open basin in the absence of wall effects will allow for a simpler identification of the pitch resonant period and damping ratio in both flap orientations. Another option that could be explored is shifting the pitch resonant period by either applying external linear springs to the device or by changing the center of gravity for continued experiments in the wave tank. Updates to the model itself may also investigate the size and location of the flap window and adjusting mass properties using the ballast ports already constructed. The goal will be to tune the device's hydrodynamics to shift its resonant pitch frequency to match the wave-excitation frequency for maximum power extraction in operational sea states, and shed loads in extreme conditions. Options for testing combinations of the adjustable geometry control discussed in this paper with a model PTO system are currently being explored.

Acknowledgements

The first author acknowledges the support of AVANGRID Foundation, Inc. for the award of a Scholarship for Energy and Environment Postgraduate Studies in the United States. This work was supported by the U.S. Department of Energy under Contract No. DE-AC36-08GO28308 with the National Renewable Energy Laboratory. Funding for the work was provided by the DOE Office of Energy Efficiency and Renewable Energy, Water Power Technologies Office.

References

[1] N. M. Tom, M. J. Lawson, Y. H. Yu and A. D. Wright, Development of a nearshore oscillating surge wave energy converter with variable geometry, *Renewable Energy* 96 (2016) 410–424.

[2] T. Whittaker, M. Folley, Nearshore oscillating wave surge converters and the development of Oyster, *Philos. Trans. R. Soc. A* 370 (2012) 345–364.

[3] J. Lucas, M. Livingstone, M. Vuorinen, J. Cruz, Development of a wave energy converter (WEC) design tool - application to the WaveRoller WEC including validation of numerical estimates, in: *Proc. 4th Int. Conf. Ocean Energy*, Dublin, Ireland (2012).

[4] E. Ramudu, Ocean wave energy-driven desalination systems for off-grid coastal communities in developing countries, in: *Proc. IEEE Global Humanitarian Tech. Conf*. Seattle, USA (2011).

[5] R. P. F. Gomes, M. F. P. Lopes, J. C. C. Henriques, L. M. C. Gato, A. F. O. Falcao, The dynamics and power extraction of bottom-hinged plate wave energy converters in regular and irregular waves, *Ocean Eng*. 96 (2015) 86–99.

[6] D. Crooks, J. V. Hoff, M. Foley, and B. Elsaesser, Oscillating wave surge converter forced oscillation tests, *Proc. 35th Int. Conf. Ocean Offshore Arctic Eng*. (OMAE 2016), Paper no. 54660.

[7] K. Ruehl, C. Michelen, S. Kanner, M. Lawson, and Y. Yu, Preliminary verification and validation of WEC-Sim, an open-source wave energy converter design tool, *Proc. 33rd Int. Conf. Ocean Offshore Arctic Eng.* (OMAE2014), Paper no. 24312.

[8] WAMIT Version 7.2 User Manual, http://www.wamit.com; 2017.